

RESEARCH ARTICLE

VIVAS: An Ergonomic Low-Cost High-Resolution Portable Vein Finder for Phlebotomy

DIVISHA GARG¹, GAURAV KUMAR¹, HARPREET SINGH¹, PRASHANT SINGH RANA¹, SHAHID AHMAD BHAT², (Member, IEEE), SMITA PATTANAİK³, RAVIMOHAN SURYANARAYAN MAVUDURU⁴, AND NEERU JINDAL⁵

¹Department of Computer Science and Engineering, Thapar Institute of Engineering and Technology, Patiala, Punjab 147004, India

²LUT Business School, LUT University, 53851 Lappeenranta, Finland

³Department of Pharmacology, Post Graduate Institute of Medical Education and Research, Chandigarh 160012, India

⁴Department of Urology, Post Graduate Institute of Medical Education and Research, Chandigarh 160012, India

⁵Department of Electronics and Communication, Thapar Institute of Engineering and Technology, Patiala, Punjab 147004, India

Corresponding author: Shahid Ahmad Bhat (shahid.bhat@lut.fi)

This work was supported by Indian Council of Medical Research, New Delhi, in the form of a Project Grant for the proposal titled “Automated Blood Extraction Device” under Grant DHR GIA/2019/000595/PRCGIA.

ABSTRACT Locating veins accurately is a common challenge in clinical settings, particularly with patients where veins are difficult to discern. The development of effective vein visualization technology is crucial for improving patient outcomes and minimizing procedural complications. This study aimed to design, develop, and evaluate a low-cost, high-resolution portable vein finder device. It was developed using affordable components and integrated imaging technology. The device captured images of veins in challenging patient scenarios. Four conventional image enhancement techniques were initially applied to these images. Subsequently, a novel image enhancement technique is proposed. The performance of each technique was qualitatively assessed using visual representation and histogram distribution and quantitatively assessed using the peak signal-to-noise ratio and structural similarity index measure. The proposed technique significantly outperformed the conventional methods. This indicates a superior enhancement of vein visibility, confirming the effectiveness of the proposed method. Thus, the newly developed vein finder, enhanced with the proposed image enhancement technique demonstrates significant potential for clinical use. It offers a reliable solution for vein detection in patients, potentially improving treatment accuracy.

INDEX TERMS Image processing, near-infrared LEDs, phlebotomy, portable vein finder, venipuncture.

I. INTRODUCTION

Vein visualization is critical in healthcare, aiding in vascular surgery, venepuncture procedures, and blood sampling for diagnostics and treatments [1]. Improper venepuncture poses risks such as medical complications and inaccurate results, particularly challenging due to anatomical variations, as highlighted by studies such as Jacobson and Winslow and Nafiu et al. [2], [3]. Due to these risks, trained professionals like phlebotomists, doctors, or nurses draw blood from the patient's veins [4]. In most cases, people have easily

The associate editor coordinating the review of this manuscript and approving it for publication was Joewono Widjaja¹.

visible veins, which facilitates accurate and swift blood collection. However, various factors such as Body Mass Index (BMI), genetics, melanin levels, patient age, rapid weight loss, skin color, or skin thickness can pose challenges during venepuncture [5]. Hence, when a patient's veins are not visible, multiple attempts may be required, causing severe pain for the patient. To address and minimize the challenges associated with inappropriate venepuncture, vein viewer technologies have been developed to provide clear visualization of veins, commonly used as venepuncture sites [6], [7]. Several methods have been investigated for the automatic insertion of a catheter into the vein, often relying on pre-processing techniques [8], [9]. The purpose

of pre-processing is to enhance contrast, making it easier to distinguish veins from other features [10]. The literature describes various vein recognition techniques [11], [12]. The motivation behind this study stems from the conventional techniques that rely on palpation or visual inspection, which can be time-consuming, inaccurate, and particularly challenging in patients with difficult venous access. The current research endeavors to address these shortcomings by introducing an innovative vein-finding device. By leveraging cutting-edge imaging technologies and intuitive user interfaces, the proposed device aims to provide healthcare professionals with real-time, high-resolution visualization of peripheral veins. Improved vein visualization can minimize the incidence of venepuncture-related complications, such as hematoma formation, nerve injury, and medication extravasation, optimize resource utilization, and reduce healthcare costs. This paper presents the design, development, and validation of the proposed vein finder. The goal is to empower healthcare professionals with tools for safer, more efficient, and patient-centered care, enhancing patient outcomes and quality of life.

II. LITERATURE REVIEW

This section delves into the existing body of knowledge and studies related to vein visualization and vein-finding technologies in the context of phlebotomy procedures. The review encompasses relevant works on (i) Infrared (IR) and (ii) Near Infrared (NIR) imaging techniques, image processing algorithms, and previous attempts to create cost-effective vein visualization systems.

Wieringa et al. discussed a non-invasive vein detection device [13]. Zhao et al. studied hand vein image acquisition and pattern detection techniques [14]. Fukuroku et al. demonstrated the effectiveness of infrared visualization in practicing venepuncture. It described the numerous advantages of using infrared light in vein detection [15]. Oliveira et al. introduced a portable and convenient vein detector to aid medical practitioners in hospitals [16].

Recently, NIR technology has gained considerable attention as a non-invasive and efficient method for imaging subcutaneous veins. Juric et al. developed an affordable mobile solution for subcutaneous vein detection via NIR spectroscopy [17]. Marathe et al. showed that NIR imaging can minimize errors in puncturing the correct vein by highlighting superficially located veins [18]. Barreras et al. revealed that using a NIR device can significantly increase the success rates of intravenous access compared to visualization or palpation, achieving 26% v/s 19.6%, respectively [19]. Ayoub et al. utilized a combined approach of a high-resolution NIR camera, a vein warmer, and Contrast Limited Adaptive Histogram Equalization (CLAHE) as an image contrast enhancer to enhance the visualization of superficial veins [20]. Tran et al. also used the NIR technique to construct a vein finder [21]. Dorotic et al. verified the performance of the transillumination devices namely

VeinViewer Flex, AccuVein AV400, and ICEN IN-G090-2, and stated that opting for a smaller device with extended battery life and reduced charging time would be a preferable choice for phlebotomy units [22].

Francisco et al. developed a low-cost, real-time NIR router for cannulation. This device featured three LED lights with a wavelength of 960nm and a CMOS-IR sensor camera combined with image processing software. The effectiveness of this device was evaluated through tests conducted at two locations: the arm and dorsal hand, considering variables such as gender, age, BMI, skin color, and arm circumference. Digital and visual imaging comparisons of vein visibility demonstrated the device's capability to accurately identify veins in real-time at both test sites [23].

Tang et al. focused on enhancing vein detection through color skin images, leveraging a fully convolutional network that includes a dilated convolution and a transposed convolution module. This architecture is specifically optimized for execution on NVIDIA's Jetson TX2, illustrating the practical application of embedded Artificial Intelligence (AI) technologies in medical devices. Their method, which features a combined loss function to refine learning outcomes, significantly advances the accuracy and efficiency of vein localization in clinical settings [24].

Kuthiala et al. employed Adaptive Histogram Equalization (AHE) and CLAHE techniques as a pre-processing step to enhance the task of segmentation. The authors found that outcomes of image segmentation after applying these techniques were most effective [25]. In recent research conducted by Quan et al., a handheld vein detection system utilizing NIR illumination is proposed [1].

Leipheimer et al. made recent advancements in robotic-assisted medical procedures by presenting a significant development VeniBot, a handheld robotic device designed for peripheral catheterization. This device combines ultrasound imaging and miniaturized robotic control to enhance the precision and success rates of catheter insertions. The device achieved first-attempt success rates of 97% for vessel punctures and 89% for sheath cannulations on tissue-mimicking models. This innovation demonstrates the potential for robotic systems to improve clinical outcomes. The findings suggest that such technologies could significantly reduce patient discomfort in challenging patient populations while ensuring high success rates in venepuncture [26].

Biradar et al. developed a non-invasive human vein detector utilizing NIR technology alongside a Raspberry Pi and a NoIR camera. The study also explored image-processing techniques namely median filtering, histogram equalization, and adaptive thresholding to improve vein visualization. The authors claim that this vein finder system is an effective solution for safe and precise blood sampling [27].

Salcedo et al. developed an edge AI-based vein detector optimized for use in the antecubital fossa. Their study introduces a novel NIR-based forearm vein segmentation dataset consisting of 2,016 labeled images. Furthermore, the authors modified the U-Net architecture to specifically

TABLE 1. Cost of available vein viewers in the market.

Author (Year) / Device	Cost (\$)
Cuper et al. (2010) [29]	10068
Vein Finder VF [30]	4000-7000
Vein Viewer ZD200 [31]	1679
VT et al. (2021) [32]	500
IISM VPism-C Phlebology [33]	3323
Vein Finder V-Pink [34]	1207
Veineux AR100 [35]	2740-3425
Vein Locator BS2000+ [36]	5035
Vensite [37]	4627
VeinViewer Flex [22]	4531-8055
AccuVein AV400 [22]	6635
ICEN IN-G090-2 [22]	2000
Quan et al. (2022) [1]	300
Proposed Device VIVAS	151

locate veins in the antecubital fossa, achieving notable precision. The model is deployed on a Raspberry Pi within a custom-built, portable vein finder device. The experimental results show the model's capability to operate efficiently for real-time, on-site vein detection [28].

A. GAPS IN THE LITERATURE

By analyzing the literature, the gaps in the existing research have been identified and the potential contributions of our proposed vein finder in improving the accuracy and efficiency of venous access during phlebotomy are highlighted.

The device proposed by Wieringa et al. is quite complicated and requires costly equipment including bulky illumination setups and multiple sensors or cameras [13]. The images Zhao et al. used are very low-quality [14]. The utilization of the commercially accessible vein finder by Juric et al. is constrained due to its high cost [17]. The vein detector introduced by Lima-Oliveira et al. is highly expensive and unaffordable for individual practitioners [16]. The vein finder developed by Tran et al. is non-portable as it consists of multiple wired connections [21]. The authors Dorotic et al. found that the VeinViewer Flex is quite large, heavy, and has a short span of battery life. AccuVein AV400 failed to present the image captured when the device was under direct sunlight. In addition, these devices come at a considerable cost. Moreover, the authors tested the performance of the device on a subject with normal BMI and forearm circumference which is a potential limitation of the study as the performances might vary on diverse populations [22]. There aren't any crucial supportive elements such as illustrative figures or diagrams that substantiate the claims made about the design and operational efficacy of the human vein detector developed by Birardar et al. Additionally, the absence of detailed descriptions of the testing environments casts doubts on the reliability and applicability of the vein finder in clinical settings [27].

For further analysis, the cost of the available vein finders in the market is tabulated in Table 1.

Consequently, it becomes crucial to explore cost-effective solutions for healthcare in low and middle-income countries.

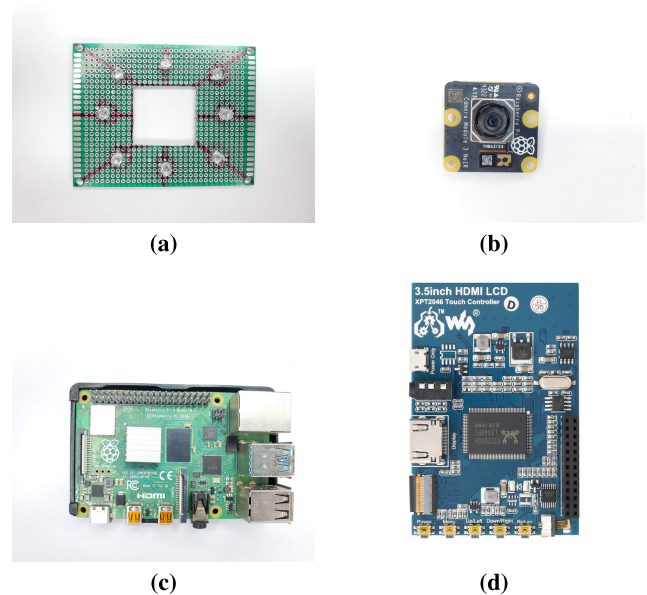


FIGURE 1. (a) NIR Array (b) Raspberry Pi Camera Module Version 3 (c) Raspberry Pi 4B (d) 3.5" Touchscreen LC.

In this context, the current research presents a simple, easy-to-use, low-cost, high-resolution, and portable vein finder capable of displaying real-time venous images by using near-infrared light.

III. DESIGN OF A VEIN IMAGING VISUALIZATION AND SCANNING (VIVAS) DEVICE

This section outlines the methodology employed to develop the vein finder VIVAS which utilizes a Raspberry Pi 4 model B 4GB variant as its primary processing unit. It incorporates a Raspberry Pi camera module Version 3 (V3) with NoIR, featuring a high-definition 12-Megapixel (MP) Sony IMX708 image sensor with a 76° viewing angle, and an improved low-light sensitivity NIR camera. This camera module V3 includes autofocus capability for image focus adjustment without manual intervention. A 3.5-inch touch LCD screen enables direct monitoring of the camera's output. To enhance vein visibility, an array of 940nm wavelength NIR LEDs surrounds the camera module. These LEDs illuminate upon device activation, improving vein visualization. The absence of an IR block filter in the camera module designates it as "NoIR," projecting veins onto the display screen. The device operates in real-time, providing continuous live footage of veins, and can be connected to an external monitor for expanded viewing. The device is supported by an onboard rechargeable battery. The Computer-Aided Design (CAD) rendering of VIVAS was created using Fusion360. Figure 1 displays the components described above for designing VIVAS. The overall methodology adopted in the current study is depicted through a block diagram in Figure 2. It illustrates that the initial phase of the process involves the activation of the NIR light source, which emits NIR light onto the skin's surface. This emitted light interacts with the blood's hemoglobin leading to a unique phenomenon where the

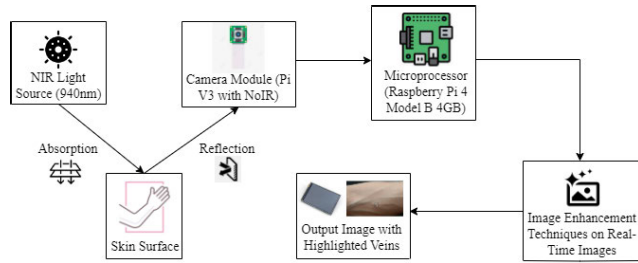


FIGURE 2. Block Diagram of the Proposed Methodology.

venous system becomes visible. This imagery is captured by a NoIR camera board seamlessly integrated with a Raspberry Pi microprocessor. The captured image is then transmitted to a computer for a subsequent enhancement process. The culmination of these image-processing steps results in an improved and refined image of the venous system. The final output can be displayed on a screen for visual examination.

VIVAS has been specifically designed with user-friendliness in mind, featuring intuitive physical buttons that simplify the operation process. A power on/off button that ensures easy activation and deactivation of the device. A dedicated button to start or launch the vein-finding application, making the operation straightforward even for novices. A button for capturing and recording images/videos, which allows users to easily document the procedure without requiring specialized skills. A control for the NIR LEDs and their illumination, which can be adjusted effortlessly to enhance image quality under various conditions. These design elements make the technology accessible and easy to use for individuals without technical training.

A. DEVELOPMENT OF VIVAS

A total of three versions of VIVAS were meticulously crafted and iteratively improved upon, guided by feedback from healthcare professionals, engineers, and end-users. Each version incorporated the overarching goal of maximizing vein visualization accuracy, operational efficiency, and clinical utility. This section provides a comprehensive overview of these versions, detailing their technical specifications, and iterative design. Through a systematic examination of each version's strengths, limitations, and performance characteristics, we aim to elucidate the evolution of our device from its conceptualization to its current state of development.

During the initial stage, the version of the device was constructed using the NIR 5MP OmniVision camera [25]. The prototype performed well but its size was rather large. Later, a second version was built utilizing IR light sources for vein detection. However, the resulting device exhibited inefficiencies in its operation. The images from this version lacked clear visibility of veins and the IR lights led to excessive illumination in the scanning area. Consequently, further efforts were invested to create an ergonomic version that would offer enhanced efficiency and be small in size.

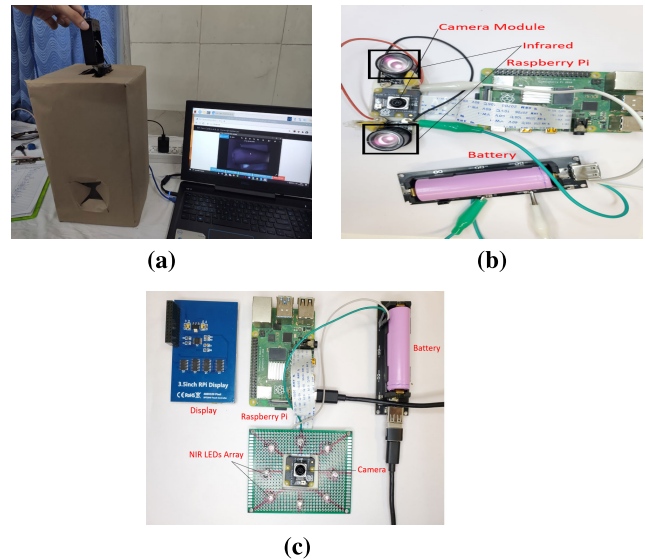


FIGURE 3. (a) First Version of VIVAS (b) Second Version of VIVAS (c) Third Version of VIVAS.

These endeavors materialized in a final version, employing NIR light sources. Figure 3 demonstrates all three versions. The 3D-printed casing designed for VIVAS is showcased in Figure 4a and the integrated device within its 3D-printed enclosure is provided in Figure 4b and Figure 4c. The snapshots of the working device are presented in Figure 5.

The final architecture of the study is represented in Figure 6. The study follows a structured approach consisting of five key steps. Firstly, the setup involves configuring three versions of VIVAS hardware. Following this, data is collected in the form of images through these versions. Subsequently, the acquired images undergo visualization and pre-processing. In the fourth step, image enhancement techniques are applied to the pre-processed images. Finally, the performance of these techniques is evaluated using both qualitative and quantitative measures, forming the conclusive step of the study's methodology.

IV. IMAGE ENHANCEMENT

Image enhancement is the process of improving the quality or visual clarity of an image through various algorithms or techniques. The initial algorithmic step involves converting the Red Green Blue (RGB)-mode image into grayscale to streamline the intricacy of image processing. After this conversion, the grayscale images are then subjected to Python-based processing, resulting in enhanced clarity of the veins. The utilized algorithms offer the advantage of increasing the contrast and sharpness of the captured images with controllable contrast stretching limits. The resultant image holds the potential as an aid during procedures involving cannulation.

This section explores four conventional and a novel image enhancement techniques described in the subsequent subsection.

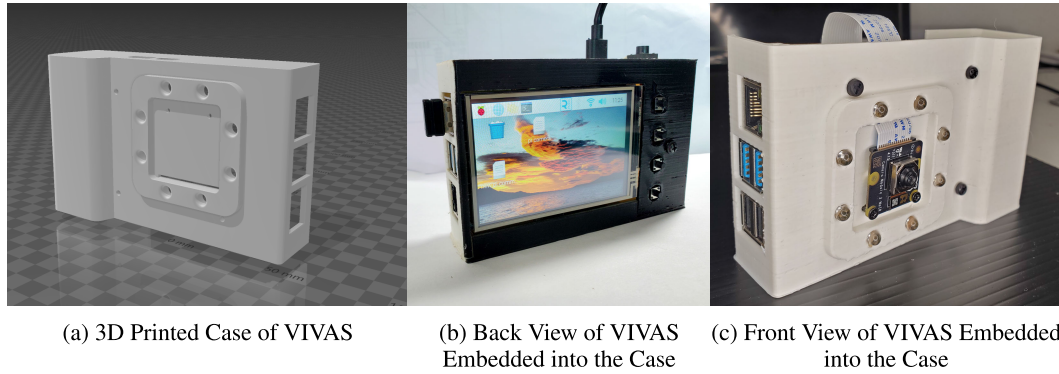


FIGURE 4. Integration of VIVAS with its dedicated 3D-Printed Casing.

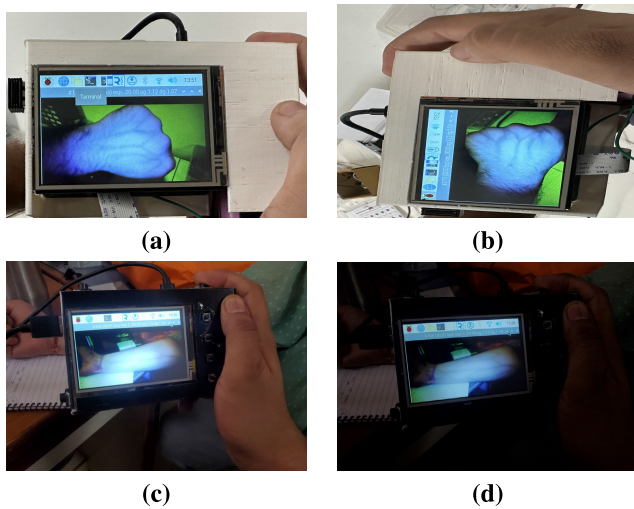


FIGURE 5. (a) Landscape View of the Working Device (b) Portrait View of the Working Device (c) Working Device in Extreme Daylight (d) Working Device in Dark.

A. BRIGHTNESS PRESERVING BI-HISTOGRAM EQUALIZATION (BPBHE)

Brightness Preserving Bi-Histogram Equalization (BPBHE) is an image enhancement technique that aims to improve the contrast of an image through bi-histogram equalization while preserving its overall brightness [38]. The transformation function $T(x, y)$ for BPBHE is given by:

$$CDF_{out}(f(x, y)) \times (L - 1) \quad \text{if } f(x, y) \leq \frac{1}{2}M$$

$$CDF_{out}(f(x, y) + \frac{1}{2}M) \times (L - 1) \quad \text{if } f(x, y) > \frac{1}{2}M \quad (1)$$

where $f(x, y)$ is the pixel intensity value at coordinates (x, y) in the input image, CDF_{out} is the Cumulative Distribution Function (CDF) of the output image, L denotes the total number of intensity levels, and M is the midpoint intensity level, which is given by:

$$M = \frac{L - 1}{2} \quad (2)$$

B. CLIPPED LOCAL ADAPTIVE HISTOGRAM EQUALIZATION (CLAHE)

Clipped Local Adaptive Histogram Equalization (CLAHE) is an image enhancement technique that improves contrast by dividing the image into small regions and applying histogram equalization independently to each region. Additionally, CLAHE includes a clipping mechanism to prevent excessive amplification of noise [39]. The transformation function $T(x, y)$ for CLAHE is given by:

$$CDF_{N_{xy}}(f(x, y)) \times (L - 1) \quad \text{if } CDF_{N_{xy}}(f(x, y)) \leq C_{max}$$

$$C_{max} \times (L - 1) \quad \text{otherwise} \quad (3)$$

where $CDF_{N_{xy}}(f(x, y))$ represents the CDF of the neighborhood N_{xy} centered around the pixel intensity value $f(x, y)$ at coordinates (x, y) in the input image, L stands for the total number of intensity levels in the image, and C_{max} is a predefined maximum limit on the CDF to prevent excessive amplification of intensities. Typically, C_{max} is set to a fraction of the total number of pixels in the neighborhood.

C. ADAPTIVE HISTOGRAM EQUALIZATION (AHE)

Adaptive Histogram Equalization (AHE) is an image enhancement technique that improves contrast by dividing the image into non-overlapping tiles or blocks and applying histogram equalization independently to each tile [25]. The transformation function $T(x, y)$ for AHE is given by:

$$T(x, y) = CDF_{N_{xy}}(f(x, y)) \times (L - 1) \quad (4)$$

where $CDF_{N_{xy}}(f(x, y))$ denotes the CDF of the neighborhood N_{xy} centered around the pixel intensity value $f(x, y)$ at coordinates (x, y) in the input image, and L represents the total number of intensity levels in the image.

D. EXPOSURE BASED SUB IMAGE HISTOGRAM EQUALIZATION (ESIHE)

Exposure-based Sub Image Histogram Equalization (ESIHE) is a method for enhancing low-contrast images. It aims to improve contrast and brightness by applying histogram equalization to each sub-image independently, taking into account the exposure variations in different parts of the

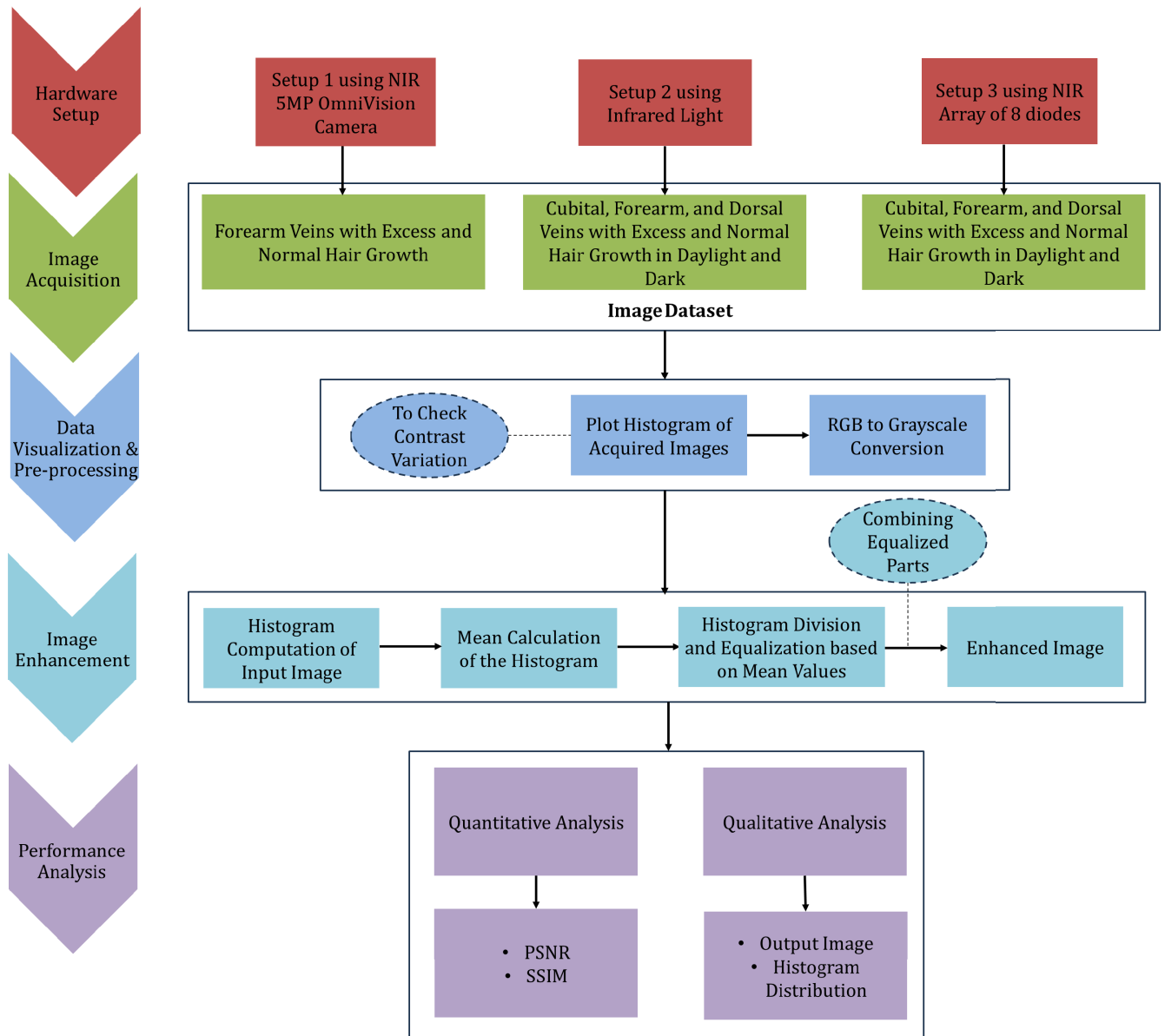


FIGURE 6. Descriptive Outline of the Study.

image. This method helps to preserve local details and prevents over-enhancement of contrast, resulting in a more visually appealing and balanced image. It maintains the original brightness characteristics of the image, avoiding any distortion in the overall illumination and appearance [40].

E. PROPOSED APPROACH

In this study, an innovative ensemble model is developed that combines two image enhancement techniques: ESIHE and CLAHE. The integration of these techniques into a single ensemble model is governed by a weighted voting system. In the implementation, ESIHE is assigned a higher weight of 0.8, reflecting its primary role in enhancing the overall exposure and brightness of the images. CLAHE, assigned a lower weight of 0.2, complements this by refining contrast

and detail in localized regions. The weighted approach ensures that the strengths of both techniques are optimally utilized, resulting in balanced enhancement across images that suffer from poor lighting and contrast issues.

The decision to use these specific weights was empirically determined through extensive testing on a diverse set of images, where the combined approach consistently outperformed the individual techniques in terms of both subjective visual quality and objective metrics. The process is described in Figure 7.

V. RESULTS AND DISCUSSION

The efficacy of all three versions of VIVAS has been evaluated across various conditions using a sample of 17 subjects as outlined in Table 2. The demographic distribution of

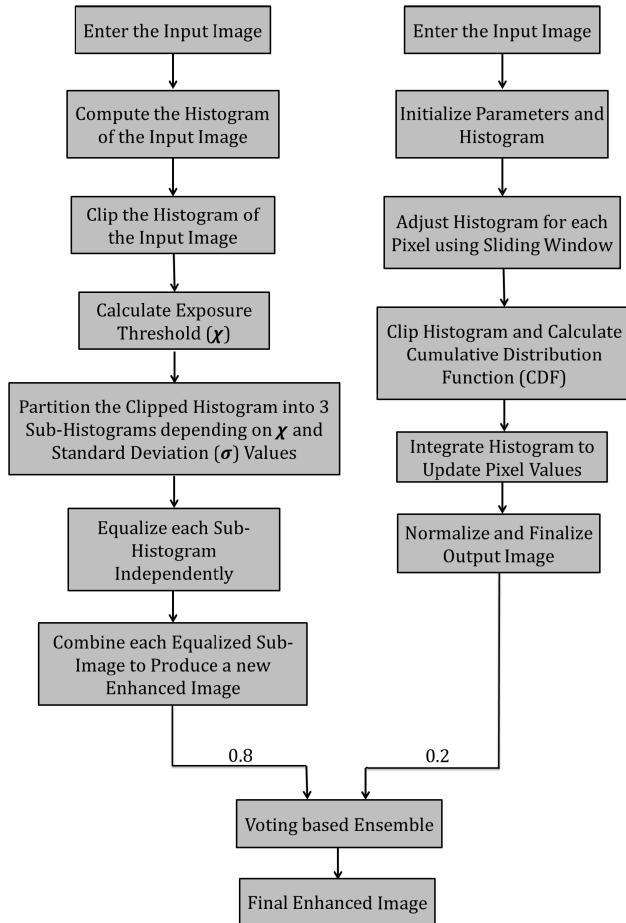


FIGURE 7. Flowchart of Proposed Technique.

TABLE 2. Total count of test subjects.

Gender	Age Group	Count
Male	19-45	10
Female	16-44	7
Total		17

these subjects is detailed in Table 3. This study reports the performance of the device on individuals with both normal and excessive hair growth under different lighting conditions. The real-time images captured and the outcomes of the image enhancement techniques for versions 1, 2, and 3 are detailed in Sections VA, 5B, and 5C, respectively.

The performance of the image enhancement techniques is assessed through both qualitative and quantitative measures. Firstly, a visual inspection of the image histograms is conducted to analyze the distribution of pixel intensities before and after enhancement. Additionally, quantitative parameters such as Peak Signal to Noise Ratio (PSNR) and Structural Similarity Index Measure (SSIM) are utilized to objectively measure the fidelity and similarity between the original and enhanced images.

- 1) *Peak Signal to Noise Ratio (PSNR)*: PSNR is calculated using the formula:

$$PSNR = 10 \cdot \log_{10} \left(\frac{MSE}{MAX^2} \right) \quad (5)$$

where:

MAX represents the maximum possible pixel value of the image.

MSE is the mean squared error between the original and enhanced images. The unit of measurement for PSNR is decibel (dB).

- 2) *Structural Similarity Index Measure (SSIM)*:

SSIM evaluates the structural similarity between images by considering luminance, contrast, and structure. It is calculated using the formula:

$$SSIM(x, y) = \frac{(2\mu_x\mu_y + c_1)(2\sigma_{xy} + c_2)}{(\mu_x^2 + \mu_y^2 + c_1)(\sigma_x^2 + \sigma_y^2 + c_2)} \quad (6)$$

where:

μ_x and μ_y are the means of the original and enhanced images, respectively.

σ_x^2 and σ_y^2 are the variances of the original and enhanced images, respectively.

σ_{xy} is the covariance between the original and enhanced images.

c_1 and c_2 are constants to stabilize the division with a weak denominator.

- 3) *Histogram Distribution*:

Histograms provide information about the range of pixel intensities present in an image and the distribution of these intensities, allowing us to assess factors such as brightness, contrast, and tonal range.

A. RESULTS OF VERSION 1

Preferential sites for venous access include the cephalic and basilic veins located in the forearm. The basilic veins arise from the merging of veins at the wrist and stand out as the prominent choice for venous access due to their size. As a result, this particular area was captured. The images were captured in a closed cardboard box with no external light. The images captured through the initial version of VIVAS and their corresponding histograms are presented in Table 4. These images are then passed to the image processing methodologies, and the results with corresponding histograms are depicted in Table 5.

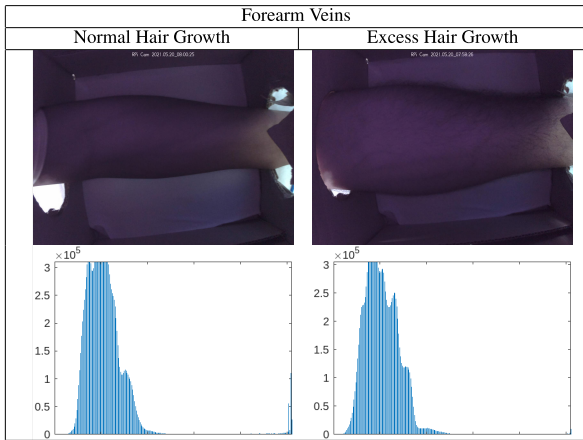
B. RESULTS OF VERSION 2

At times, it is challenging to distinguish the forearm veins from the radial artery. In that case, dorsal metacarpal veins are the preferred choice for cannulation. Dorsal metacarpal veins stand out due to their palpability and the support provided by metacarpal bones. However, accessing these veins could prove challenging when the skin is thin and delicate. To address this, imaging of the hand dorsal region is conducted. Also, accessing the antecubital vein poses a recurrent challenge for medical practitioners due to

TABLE 3. Test subject demographics for the proposed device.

Age			Body Mass Index				Hair Growth			Skin Color	
Adolescent	Young Adults	Middle-aged Adults	Underweight	Normal	Overweight	Obese	No	Normal	Excess	Fair	Dark
1	14	2	5	5	6	1	5	8	4	12	5

TABLE 4. Images captured by version 1 and their corresponding histograms.



factors such as patient characteristics and varying anatomical features. Thus, the selected locations include hand dorsal veins, forearm veins, and veins in the cubital fossa region. The efficacy of the second version is evaluated in both daylight and a dark room. The original images and their histogram distributions are presented in Table 6. The captured images are subsequently processed using image processing methodologies. The outcomes of these methodologies with corresponding histograms are presented in Table 7. The column “Image 1” displays the enhanced images of cubital veins, “Image 2” showcases enhanced images of dorsal veins with excess hair growth, “Image 3” displays enhanced images of dorsal veins with normal hair growth, and “Image 4” features enhanced images for forearm veins.

C. RESULTS OF VERSION 3

The selected sites encompass the dorsal veins of the hand, forearm veins, and antecubital veins. The performance evaluation of the third version is also conducted under both daylight and low-light conditions. Original images and their histogram distributions are displayed in Table 8. Following image capture, processing occurs using image processing methodologies. The results of these processes along with corresponding histograms are outlined in Table 9. The column “Image 1” displays the enhanced images of cubital veins, “Image 2” showcases enhanced images of dorsal veins with excess hair growth, “Image 3” displays enhanced images of dorsal veins with normal hair growth, and “Image 4” features enhanced images for forearm veins.

To provide a comprehensive overview, Table 10 provides detailed descriptions of the test cases used to evaluate the performance of the three versions of VIVAS.

TABLE 5. Results of enhancement techniques on images captured by version 1 and their corresponding histograms.

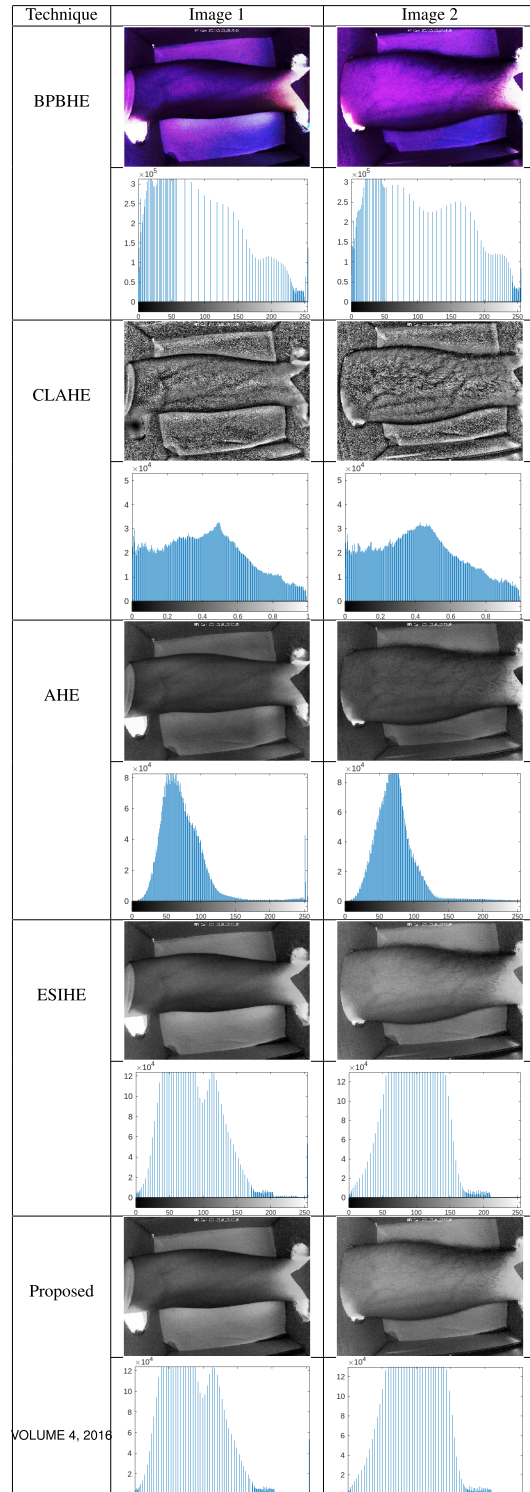




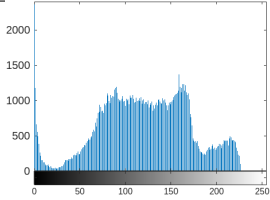
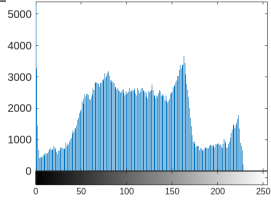
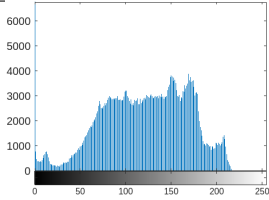
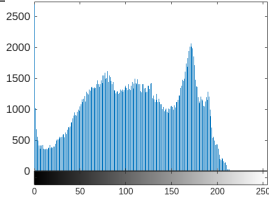


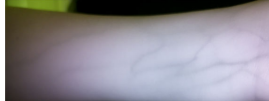

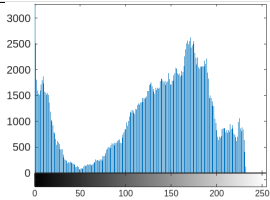
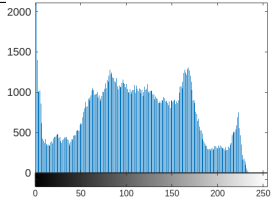
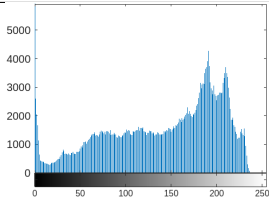
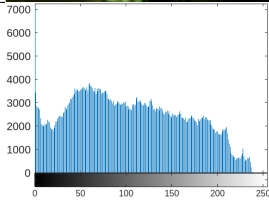
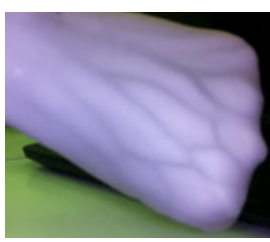

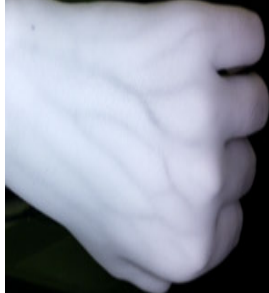
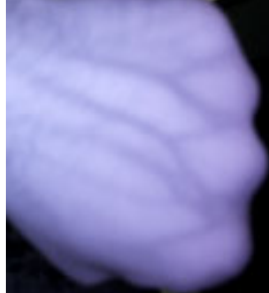
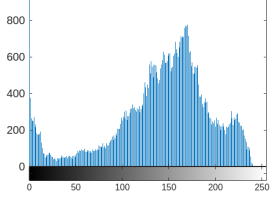
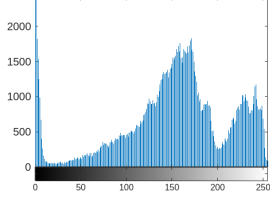
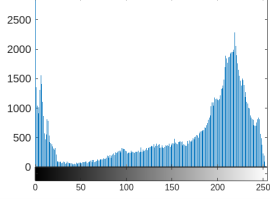
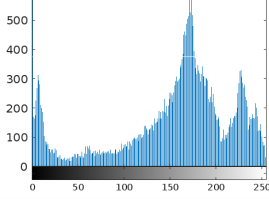


TABLE 6. Images captured by version 2 and their corresponding histograms.

Environment	Daylight		Dark	
Hair Growth / Body Region	Normal	Excess	Normal	Excess
Antecubital Veins				
				
Forearm Veins				
				
Hand Dorsal Veins				
				

Each test case specifies the conditions under which the investigation of the device was done, including lighting conditions and anatomical regions. Tables 11, 12, and 13 then presents the performance metrics (PSNR and SSIM values) for each test image, offering a comparative analysis of the results across versions 1, 2, and 3, respectively.

D. INTERPRETATION OF RESULTS

This section aims to find the most optimal version of VIVAS and image enhancement technique based on PSNR and SSIM values presented in Tables 11, 12, and 13 across all the

testing conditions. The PSNR and SSIM values for all the enhancement techniques are compared for each image in every version of VIVAS. The image enhancement technique that outputs the highest PSNR value for each image is recorded as the most optimal. The highest value indicates that under the given condition, a particular enhancement technique performs well. This approach allows us to illustrate the strengths of each technique under specific scenarios. It also allows to compare the three versions of VIVAS. The version that exhibits the highest values for PSNR and SSIM across all the varying conditions is chosen as the most optimal for detecting difficult veins. The image-wise analysis is detailed in the subsequent subsection.

TABLE 7. Results of enhancement techniques on images captured by version 2 with their corresponding histograms.


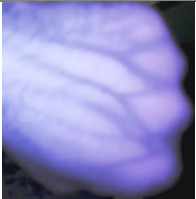


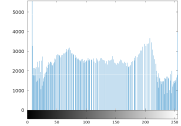
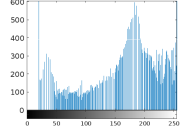
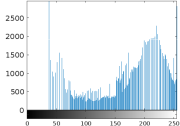
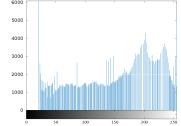
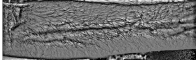

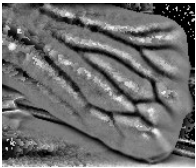
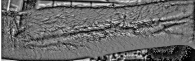
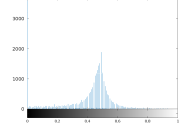
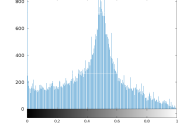
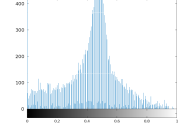
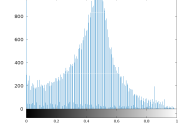




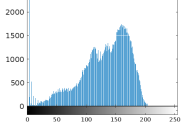
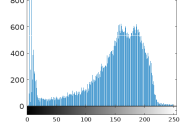
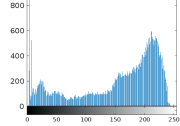
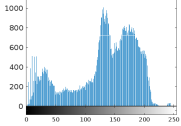

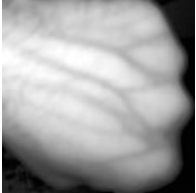


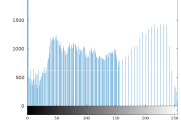
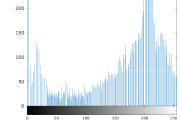
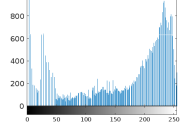
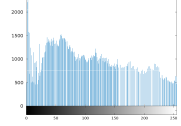

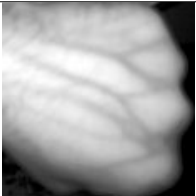


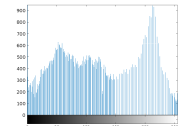
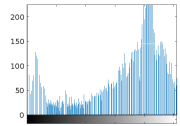
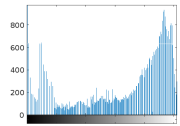
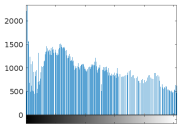
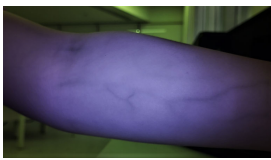



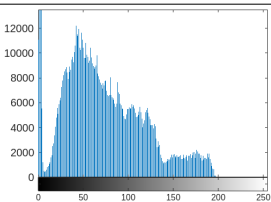
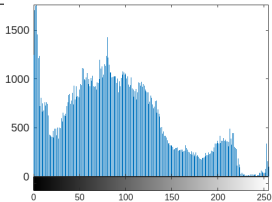
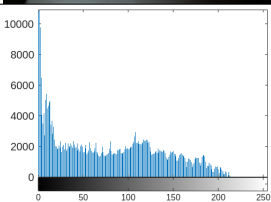
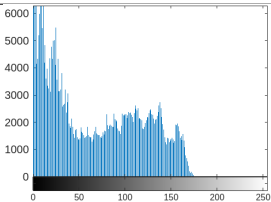



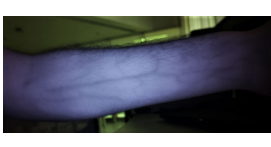
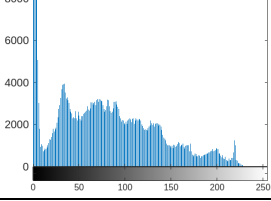
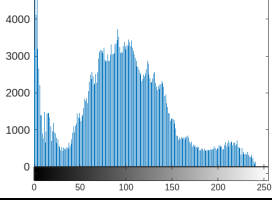
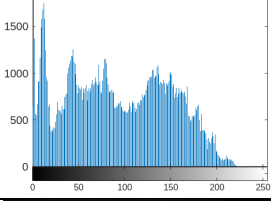
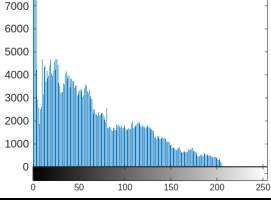
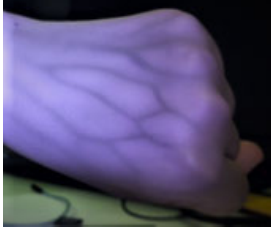



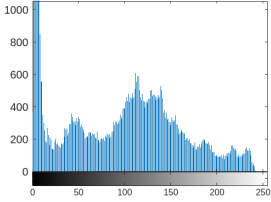
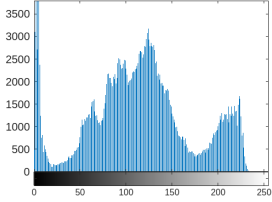
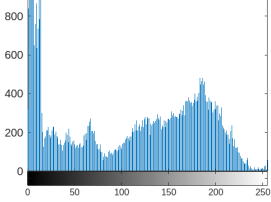
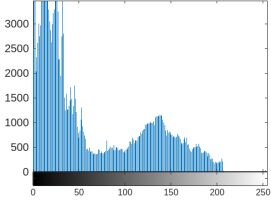
Technique	Image 1	Image 2	Image 3	Image 4
BPBHE				
				
CLAHE				
				
AHE				
				
ESIHE				
				
Proposed				
				

TABLE 8. Images captured by version 3 and their corresponding histograms.

Environment	Daylight		Dark	
Hair Growth / Body Region	Normal	Excess	Normal	Excess
Antecubital Veins				
				
Forearm Veins				
				
Hand Dorsal Veins				
				

1) ANALYSIS OF BPBHE

The results of BPBHE depict that the risk of vein pattern distortion due to uneven brightness adjustments is mitigated. It can be observed from Table 12 and 13 that the PSNR values for BPBHE in both versions 2 and 3 of VIVAS for images 2, 6, and 8 are high. For version 2, high PSNR values are 24.3262 dB for image 2, 25.7414 dB for image 6, and 23.4001 dB for image 8. For version 3, high PSNR values are 28.7459 dB for image 2, 27.5403 dB for image 6, and 25.8637 dB for image 8. Additionally, for version 2, high PSNR values are also observed for image 11 (20.8148 dB) and image 12 (21.4948 dB). The

conditions for these images are detailed in Table 10. From these observations, it can be concluded that BPBHE performs particularly well for the dorsal veins with excess hair growth in both dark and daylight and forearm veins with normal hair growth in a dark room. Furthermore, BPBHE shows robust performance for version 2 for both dorsal and forearm veins with normal hair growth in daylight. However, it is less effective for forearm veins with excess hair growth and cubital veins under any hair growth level or lighting condition.

Now, if the PSNR and SSIM values of BPBHE for all three versions are compared, it can be seen that the values

TABLE 9. Results of enhancement techniques on images captured by version 3 with their corresponding histograms.





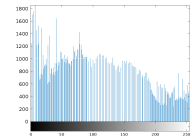
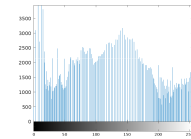
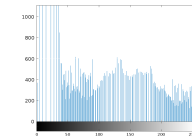
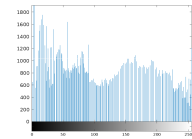


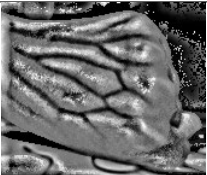

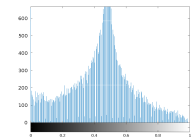
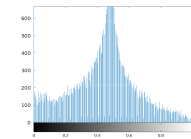
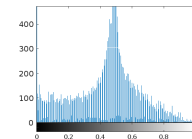
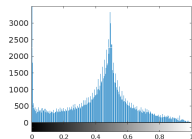




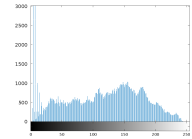
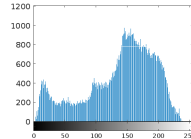
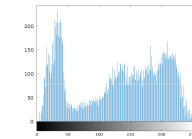
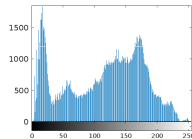




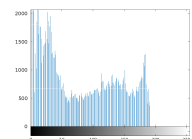
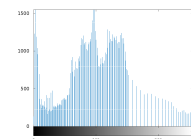
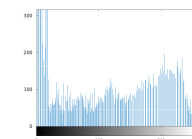
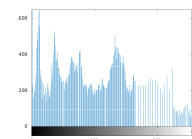

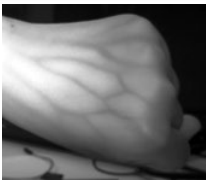


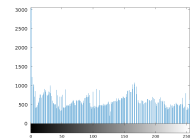
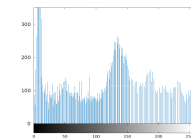
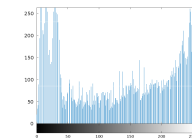
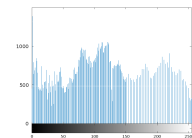
Technique	Image 1	Image 2	Image 3	Image 4
BPBHE				
				
CLAHE				
				
AHE				
				
ESIHE				
				
Proposed				
				

TABLE 10. Description of the test cases for VIVAS versions.

Version	Image Number	Image Description
Version 1	Image 1	Forearm Veins with Normal Hair Growth
	Image 2	Forearm Veins with Excess Hair Growth
Version 2 and Version 3	Image 1	Cubital Veins with Excess Hair Growth in Dark Room
	Image 2	Dorsal Veins with Excess Hair Growth in Dark Room
	Image 3	Forearm Veins with Excess Hair Growth in Dark Room
	Image 4	Cubital Veins with Normal Hair Growth in Dark Room
	Image 5	Dorsal Veins with Normal Hair Growth in Dark Room
	Image 6	Forearm Veins with Normal Hair Growth in Dark Room
	Image 7	Cubital Veins with Excess Hair Growth in Daylight
	Image 8	Dorsal Veins with Excess Hair Growth in Daylight
	Image 9	Forearm Veins with Excess Hair Growth in Daylight
	Image 10	Cubital Veins with Normal Hair Growth in Daylight
	Image 11	Dorsal Veins with Normal Hair Growth in Daylight
	Image 12	Forearm Veins with Normal Hair Growth in Daylight

for version 3 are higher than those of versions 1 and 2. This depicts the efficacy of version 3 over other versions.

2) ANALYSIS OF CLAHE

The veins are visible in the images processed with CLAHE for all the developed versions of VIVAS. This indicates some level of success in enhancing vein visibility through CLAHE. However, despite the visual clarity of the veins, it’s important to note that the PSNR and SSIM values obtained for all conditions were consistently low. For example, the PSNR values for all three versions ranged from 3.5986 dB (lowest for image 5 in version 2) to 14.2922 dB (highest for image 2 in version 1) while the SSIM values ranged from 0.0164 (lowest for image 1 in version 1) to 0.1934 (highest for image 4 in version 3). This discrepancy between visual perception and quantitative metrics suggests that while CLAHE may improve vein visibility to some extent, it does so at the expense of overall image quality. By viewing the results of CLAHE, it is examined that artifacts are introduced in the images due to excessive histogram equalization.

3) ANALYSIS OF AHE

In the context of medical imaging applications, the issues of contrast variations within images arising from fluctuating lighting conditions are resolved by AHE. Observations reveal that by using the AHE technique, the quality of images has improved. It has enhanced both dark as well as bright areas, making images more visually clear.

It can be noted from Table 11 that for the first version of VIVAS, the technique attained the highest PSNR and SSIM values for both image 1 (PSNR=19.2065 dB, SSIM=0.7578) and image 2 (PSNR=17.8521 dB, SSIM=0.7236). For the

second version of VIVAS, it is perceived from Table 12 that the high value achieved is for image 4 and image 10 with PSNR values of 20.6338 dB and 20.3648 dB, respectively. Concerning Table 10, it is thus certain that the technique enhanced the visibility of forearm veins with both normal and excess hair growth in version 1. The technique improved the clarity of vein detection only in cubital veins with normal hair growth scenarios in both dark and daylight conditions for version 2. For the third version of VIVAS, the technique exhibited average performance across all test conditions, with PSNR values ranging from 18.6381 dB (lowest for image 1) to 24.5055 dB (highest for image 12) and SSIM values ranging from 0.6908 (lowest for image 2) and 0.8463 (highest for image 6). Thus, AHE falls short of achieving consistent vein visibility across diverse conditions.

When comparing the PSNR and SSIM values of the AHE technique across all images among versions 1 (Table 11), 2 (Table 12), and 3 (Table 13), it is noted that version 3 generally achieves higher PSNR and comparable SSIM values than the other two versions, demonstrating the superior performance of version 3.

4) ANALYSIS OF ESIHE

It can be inspected from Tables 12 and 13 that except for image 8, ESIHE consistently yielded better results than the conventional image enhancement techniques across all test conditions whether in dark, daylight, or scenarios involving varying levels of hair growth achieving the high SSIM value of 0.9823 for image 3 in version 2 and 0.9853 for image 7 in version 3 of VIVAS. This suggests that it is unable to enhance dorsal veins with excess hair growth in daylight conditions. Otherwise, it independently enhanced the contrast and brightness of each localized sub-image within the original image by preserving the local details. This reveals that enhanced vein visibility provided by ESIHE may improve patient outcomes and reduce procedural complications.

Even though the SSIM values for this technique in both versions 2 and 3 are high across all conditions, a comparison reveals that the SSIM values for version 3 are higher than other versions. Additionally, the PSNR values for version 3 are also consistently higher than the other two. This indicates that the performance of version 3 is superior to that of version 2.

5) ANALYSIS OF PROPOSED TECHNIQUE

In the initial version of the vein finder development, the proposed novel image enhancement technique demonstrated favorable results (Table 11), although it did not achieve the highest PSNR and SSIM values compared to AHE. Specifically, the novel technique scored a PSNR of 17.102 dB for image 1 and 15.1515 for image 2 and an SSIM of 0.7245 for image 1 and 0.653 for image 2, which were satisfactory but slightly lower than those achieved by AHE. Achieving near-comparable results indicates that the novel

TABLE 11. PSNR and SSIM values for version 1.

	PSNR (dB)(↑)					SSIM(↑)				
	BPBHE	CLAHE	AHE	ESIHE	Proposed	BPBHE	CLAHE	AHE	ESIHE	Proposed
Image 1	13.0281	12.4734	19.2065	14.999	17.102	0.5156	0.0164	0.7578	0.6913	0.7245
Image 2	11.4434	14.2922	17.8521	12.451	15.1515	0.456	0.0176	0.7236	0.5825	0.653

TABLE 12. PSNR and SSIM values for version 2.

	PSNR (dB)(↑)					SSIM(↑)				
	BPBHE	CLAHE	AHE	ESIHE	Proposed	BPBHE	CLAHE	AHE	ESIHE	Proposed
Image 1	19.9406	6.6507	19.3502	21.6107	21.7748	0.904	0.0185	0.7975	0.9349	0.9356
Image 2	24.3262	4.621	19.1165	20.1356	25.2156	0.8834	0.0454	0.8068	0.9155	0.9316
Image 3	22.8623	6.9334	19.6295	26.2577	26.3976	0.935	0.0369	0.7657	0.9823	0.9824
Image 4	19.0477	6.4152	20.6338	19.4588	21.3344	0.8304	0.0609	0.7592	0.9143	0.9168
Image 5	20.8336	3.5986	18.3863	26.8867	27.2188	0.7597	0.0903	0.7066	0.9026	0.9535
Image 6	25.7414	4.8025	21.7853	21.6221	26.532	0.8782	0.0667	0.8387	0.9512	0.9579
Image 7	20.6528	7.2491	18.9702	21.7647	21.8021	0.8848	0.0472	0.767	0.9011	0.902
Image 8	23.4001	5.0846	19.9941	17.5923	24.5949	0.8641	0.0701	0.7969	0.8614	0.8804
Image 9	21.3646	7.0469	19.7637	22.2438	22.3155	0.9017	0.0368	0.7952	0.9316	0.9317
Image 10	19.8518	6.74	20.3648	19.7249	21.5821	0.8268	0.0729	0.8245	0.8889	0.8942
Image 11	20.8148	5.114	19.1144	19.3085	21.354	0.8461	0.0397	0.7758	0.8983	0.9109
Image 12	21.4948	5.3503	20.2585	19.5032	22.4862	0.8626	0.0252	0.8178	0.9346	0.9382

TABLE 13. PSNR and SSIM values for version 3.

	PSNR (dB)(↑)					SSIM(↑)				
	BPBHE	CLAHE	AHE	ESIHE	Proposed	BPBHE	CLAHE	AHE	ESIHE	Proposed
Image 1	24.4808	9.8508	18.6381	24.5022	24.5467	0.9317	0.092	0.7873	0.9847	0.9892
Image 2	28.7459	10.0213	19.086	26.8422	29.0395	0.9348	0.0479	0.6908	0.962	0.9794
Image 3	24.6389	10.6333	19.6925	28.5716	28.5895	0.8895	0.127	0.7597	0.9833	0.9927
Image 4	22.2936	8.9765	21.9032	29.9542	30.3692	0.7767	0.1934	0.8435	0.9769	0.995
Image 5	23.5515	6.0708	22.2995	31.31	31.4338	0.8772	0.053	0.7658	0.9825	0.9964
Image 6	27.5403	7.624	22.0492	26.7095	28.8573	0.9538	0.0212	0.8463	0.9726	0.9831
Image 7	23.1831	8.5096	19.7622	28.0283	28.4438	0.9334	0.0374	0.7562	0.9853	0.9897
Image 8	25.8637	7.1447	20.2483	22.2213	26.0745	0.9528	0.0443	0.7206	0.9121	0.9597
Image 9	21.4346	8.1219	19.0822	31.1966	31.6097	0.9158	0.0459	0.7322	0.9792	0.9824
Image 10	22.7075	10.4082	21.7501	25.3735	25.4348	0.8996	0.0545	0.8198	0.9712	0.9749
Image 11	23.4918	8.0959	21.6098	31.9843	31.9966	0.9015	0.0637	0.7546	0.981	0.993
Image 12	23.5812	9.5091	24.5055	28.4373	28.7283	0.8849	0.1381	0.8418	0.9714	0.9877

method holds substantial potential for further refinement and optimization.

It can be observed from Table 12 that in the second version of VIVAS, the proposed novel image enhancement technique began to demonstrate its superior capabilities. Outperforming all conventional techniques, including AHE, the novel technique achieved the highest PSNR and SSIM values, with scores ranging from 21.3344 dB (lowest for image 4) to 27.2188 dB (highest for image 5) and SSIM scores ranging from 0.8804 (lowest for image 8) to 0.9824 (highest for image 3), which are significantly higher than the first version.

Table 13 illustrates that the third version resulted in the highest PSNR and SSIM scores, ranging from 24.5467 dB (PSNR lowest for image 1) to 31.9966 dB (PSNR highest for image 11) and from 0.9597 (SSIM lowest for image 8) to 0.9964 (SSIM highest for image 5), yet surpassing those of the second version, thereby establishing a clear trend of progressive improvement. The novel technique not only continued to outperform all conventional methods but also did so with increasing margins, solidifying its status as

the most effective method for enhancing vein visualization. This dramatic improvement highlights the effectiveness of the technique in leveraging the advanced capabilities of the refined hardware, making it the most suitable method for clinical use.

Table 14 summarizes the performance results of the most optimal version of VIVAS, i.e. version 3, and comparative results of image enhancement techniques as outlined in the current research. Each cell in the table is assigned a value ranging from 1 to 5, with 1 indicating the least performance and 5 representing the highest performance. The performance values for VIVAS version 3 are derived from the visual representations of the captured images, as provided in Table 8. The performance ratings for the image enhancement techniques are based on the detailed analysis provided in the above subsections. This scoring system provides a clear, quantitative comparison to facilitate an understanding of the relative efficacy of the device and each technique.

It can be observed from Table 14 that though VIVAS is sufficient for operational purposes and initial clinical application, it does not capture the cubital veins in daylight

TABLE 14. Summarized results of the article.

Body Region	Cubital				Hand Dorsal				Forearm				
	Daylight		Dark		Daylight		Dark		Daylight		Dark		
	Normal	Excess	Normal	Excess	Normal	Excess	Normal	Excess	Normal	Excess	Normal	Excess	
Environment													
Hair Growth													
VIVAS Version 3	3	5	4	5	5	5	5	5	5	5	5	4	4
BPBHE	2	2	2	2	4	4	3	4	4	2	4	2	2
CLAHE	1	1	1	1	1	1	1	1	1	1	1	1	1
AHE	4	2	4	2	2	2	2	2	2	2	5	5	5
ESIHE	4	4	4	4	4	3	4	4	4	4	4	4	4
Proposed	5	5	5	5	5	5	5	5	5	5	5	5	5

conditions much effectively. This places limitations on the resolution, aperture, and focal length of the imaging system. As part of our commitment to enhancing the capabilities of the device and addressing these limitations, future developments will consider integrating a camera with higher resolution, greater aperture, and optimal focal length. These upgrades will aim to substantially improve the quality of vein imaging, thereby enhancing the overall effectiveness and usability of the vein finder in more demanding clinical environments.

6) COMPARISON WITH THE EXISTING STUDIES

The comparative analysis highlights several key areas where our device VIVAS outperforms and addresses the limitations identified in the existing technology.

In contrast to the approach taken by [13], [21], [22], and [24] this research introduces a vein finder emphasizing simplicity. VIVAS leverages a minimalist design philosophy, utilizing an in-house developed illumination system and a single camera setup. This enhances the portability and ease of use, making it more suitable for everyday clinical practice as compared to the existing devices that need specialized training.

Contrary to the findings presented by [16], [17], [22], [24], and [26] our study suggests that economic factors play a significant role in the practical deployment and widespread adoption of such technologies. By focusing on reducing costs, we aim to address a critical barrier that has been identified in earlier research, potentially broadening the accessibility and application of these devices in resource-constrained settings. Despite its lower price, this system offers high resolution and low power consumption, presenting a viable and economically advantageous alternative to portable medical devices.

In contrast to the performance limitations of the AccuVein AV400 under sunlight [22], VIVAS presents captured images on subjects, ensuring that veins remain visible within these images despite the challenging lighting conditions. Additionally, unlike [22], the performance of VIVAS has been tested on subjects with abnormal BMI, representing a significant advantage of this study as it accounts for performance variations across diverse populations. The test results are presented in Tables 15 and 16.

The sophisticated camera setup of VIVAS maintains image clarity across various distances without requiring manual adjustment. In contrast, the basic IR CMOS camera used in [23] requires manual focusing to maintain image clarity, which can be cumbersome and less efficient in clinical settings. VIVAS uses Raspberry Pi as the core processing unit, significantly reducing its size and weight, making it self-contained and highly portable. This contrasts sharply with the existing study's reliance on a laptop for processing, which increases bulk and limits mobility, crucial factors in clinical environments. Also, VIVAS features all built-in equipment for intuitive control and operation whereas [23] relies on external power sources and display options,

TABLE 15. Test results under direct light on hard-to-find veins.












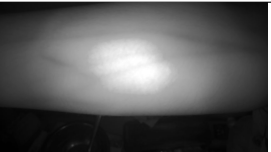


S.No.	Testing Condition	VIVAS Results	Proposed Technique Results	Metric Values
1	Dark Skinned			PSNR=37.6396 SSIM=0.9826
2	Underweight			PSNR=25.501 SSIM=0.9726
3	Overweight			PSNR=27.5482 SSIM=0.9615
4	Obese			PSNR=28.3557 SSIM=0.9783
5	Subcutaneous Fat			PSNR=26.7082 SSIM=0.9656

TABLE 16. Test results under low light on hard-to-find veins.

S.No.	Testing Condition	VIVAS Results	Proposed Technique Results	Metric Values
1	Adolescent			PSNR=27.7857 SSIM=0.9806
2	Middle-aged Adults			PSNR=28.2941 SSIM=0.9734

hindering its practical usability. Moreover, it offers limited display options as compared to VIVAS. The NIR array used in VIVAS provides more uniform illumination compared to the three LEDs used in [23], thus, enhancing vein visibility under diverse lighting conditions. With onboard storage and WiFi capabilities, VIVAS facilitates easy data storage, backup, and cloud connectivity, improving its integration into digital healthcare systems. The absence of these features in [23] restricts its functionality and fails to leverage modern digital infrastructure essential for contemporary healthcare delivery. Compared to the \$80-100 range reported by [23], the production cost of VIVAS ranges from \$40-80.

This cost reduction makes our device more economically viable.

The components used in VIVAS significantly reduce the financial barrier to deployment. In contrast, the device presented in [24] relies on the more expensive Jetson, necessitating additional expenditures for specialized deep learning development and optimization. VIVAS’s modular nature supports scalability and allows for extensive customization to meet diverse clinical needs or incorporate technological advancements without significant overhaul. Reference [24], however, shows potential restrictions in customization and scalability due to its reliance

on proprietary systems and integrated hardware-software solutions.

An important aspect of our novel image enhancement technique is its computational efficiency. Unlike many of the existing approaches [24], [26], [28] that rely on deep learning frameworks, our method achieves high-quality enhancement results without the heavy computational overhead. This not only makes our technique more accessible and feasible for real-time medical applications but also significantly reduces the dependency on high-end hardware resources. The efficiency of our approach is critical for its implementation in portable vein finder devices, where power consumption and processing speed are key constraints.

In contrast to [27], our research incorporates comprehensive illustrative figures and detailed diagrams. These visual aids provide clear evidence and validation of VIVAS's design principles and functionality, enhancing our findings' transparency and credibility. Furthermore, unlike the aforementioned study, our research includes exhaustive descriptions of the VIVAS testing environments. This additional detail ensures a thorough understanding of the performance of VIVAS under different conditions.

Thus, the enhancements and features of VIVAS not only surpass the previous studies but also significantly contribute to its potential for widespread clinical adoption. By addressing the technological and operational limitations observed in previous models, VIVAS sets a new standard for effectiveness, efficiency, and user engagement in vein detection technology.

VI. CONCLUSION

This study has successfully designed and developed a cost-effective, high-resolution portable vein finder, which utilizes an onboard microprocessor and an eight-LED NIR probe to accurately detect veins. The third version of this device emerged as the most optimal, featuring a user-friendly and robust design that enhances performance significantly. It effectively penetrates the skin non-invasively, captures images, and applies advanced image enhancement techniques to optimize vein visualization. Among these techniques, the proposed novel image enhancement technique demonstrated superior capabilities, markedly improving vein visualization compared to conventional methods. This makes the vein finder particularly valuable in medical settings requiring precise vein detection, such as during venepuncture or intravenous therapy.

VII. FUTURE SCOPE

Future work will focus on expanding the applicability of the vein finder to a more wider range of patient demographics and exploring the integration of AI to further refine image processing and enhancement techniques as performed by [28]. This continual evolution will aim to solidify the role of the proposed vein finder in improving clinical outcomes and patient care through technological innovation.

REFERENCES

- [1] P. Van Quan, P. N. Nhue, L. D. Tuan, L. H. Hai, L. A. Tu, D. N. Thuan, and T. V. Duong, "Portable hand vein finder system based on near-infrared illumination and morphological image processing," in *Proc. 8th Int. Conf. Develop. Biomed. Eng. Vietnam*, 2020, pp. 113–121.
- [2] A. F. Jacobson and E. H. Winslow, "Variables influencing intravenous catheter insertion difficulty and failure: An analysis of 339 intravenous catheter insertions," *Heart Lung*, vol. 34, no. 5, pp. 345–359, Sep. 2005.
- [3] O. O. Nafiu, C. Burke, A. Cowan, N. Tutuo, S. Maclean, and K. K. Tremper, "Comparing peripheral venous access between obese and normal weight children," *Pediatric Anesthesia*, vol. 20, no. 2, pp. 172–176, Feb. 2010.
- [4] C.-Y. Sun, K.-C. Lee, I.-H. Lin, C.-L. Wu, H.-P. Huang, Y.-Y. Lin, Y.-F. Hsu, and H.-R. Yu, "Near-infrared light device can improve intravenous cannulation in critically ill children," *Pediatrics Neonatology*, vol. 54, no. 3, pp. 194–197, Jun. 2013.
- [5] N. Ibrahim, L. K. Liang, L. Z. Zheng, L. Y. Ling, K. H. Khairulbadri, M. Mohamad, H. M. Poad, and S. Sari, "Visualization of hand vein using Raspberry Pi images in contactless vein detector," in *Proc. 12th Nat. Tech. Seminar Unmanned Syst. Technol.*, 2020, pp. 273–281.
- [6] M. J. Kim, J. M. Park, N. Rhee, S. M. Je, S. H. Hong, Y. M. Lee, S. P. Chung, and S. H. Kim, "Efficacy of VeinViewer in pediatric peripheral intravenous access: A randomized controlled trial," *Eur. J. Pediatrics*, vol. 171, no. 7, pp. 1121–1125, Jul. 2012.
- [7] P. Szmuk, J. Steiner, R. B. Pop, A. Farrow-Gillespie, E. J. Mascha, and D. I. Sessler, "The VeinViewer vascular imaging system worsens first-attempt cannulation rate for experienced nurses in infants and children with anticipated difficult intravenous access," *Anesthesia Analgesia*, vol. 116, no. 5, pp. 1087–1092, 2013.
- [8] C. Kauba, J. Reissig, and A. Uhl, "Pre-processing cascades and fusion in finger vein recognition," in *Proc. Int. Conf. Biometrics Special Interest Group*, Sep. 2014, pp. 1–6.
- [9] R. Fernández and M. Armada, "Multisensory system for the detection and localization of peripheral subcutaneous veins," *Sensors*, vol. 17, no. 4, p. 897, Apr. 2017.
- [10] A. Uhl, C. Busch, S. Marcel, and R. Veldhuis, *Handbook of Vascular Biometrics*. Cham, Switzerland: Springer, 2020.
- [11] K. Shaheed, H. Liu, G. Yang, I. Qureshi, J. Gou, and Y. Yin, "A systematic review of finger vein recognition techniques," *Information*, vol. 9, no. 9, p. 213, Aug. 2018.
- [12] S. Moccia, E. De Momi, S. El Hadji, and L. S. Mattos, "Blood vessel segmentation algorithms—Review of methods, datasets and evaluation metrics," *Comput. Methods Programs Biomed.*, vol. 158, pp. 71–91, May 2018.
- [13] F. P. Wieringa, F. Mastik, F. J. T. Cate, H. A. M. Neumann, and A. F. W. van der Steen, "Remote non-invasive stereoscopic imaging of blood vessels: First in-vivo results of a new multispectral contrast enhancement technology," *Ann. Biomed. Eng.*, vol. 34, no. 12, pp. 1870–1878, Dec. 2006.
- [14] S. Zhao, Y.-D. Wang, and Y.-H. Wang, "Biometric identification based on low-quality hand vein pattern images," in *Proc. Int. Conf. Mach. Learn. Cybern.*, vol. 2, Jul. 2008, pp. 1172–1177.
- [15] K. Fukuroku, Y. Narita, Y. Taneda, S. Kobayashi, and A. A. Gayle, "Does infrared visualization improve selection of venipuncture sites for indwelling needle at the forearm in second-year nursing students?" *Nurse Educ. Pract.*, vol. 18, pp. 1–9, May 2016.
- [16] G. Lima-Oliveira, W. Volanski, G. Lippi, G. Picheth, and G. C. Guidi, "Pre-analytical phase management: A review of the procedures from patient preparation to laboratory analysis," *Scandin. J. Clin. Lab. Invest.*, vol. 77, no. 3, pp. 153–163, Apr. 2017.
- [17] S. Juric, V. Flis, M. Debevc, A. Holzinger, and B. Zalik, "Towards a low-cost mobile subcutaneous vein detection solution using near-infrared spectroscopy," *Sci. World J.*, vol. 2014, pp. 1–15, Jul. 2014.
- [18] M. Marathe, N. S. Bhatt, and R. Sundararajan, "A novel wireless vein finder," in *Proc. Int. Conf. Circuits, Commun., Control Comput.*, Nov. 2014, pp. 277–280.
- [19] J. Barreras and T. P. Chang, "Using a near infrared device to improve successful venous access in children with special health care needs," *J. Assoc. for Vascular Access*, vol. 22, no. 2, pp. 75–80, Jun. 2017.
- [20] Y. Ayoub, S. Serhal, B. Farhat, A. Ali, J. Amatoury, H. Nasser, and M. A. Ali, "Diagnostic superficial vein scanner," in *Proc. Int. Conf. Comput. Appl. (ICCA)*, Aug. 2018, pp. 321–325.

- [21] L. T. Tran and H. T. T. Pham, "Designing and building the vein finder system utilizing near infrared technique," in *Proc. 7th Int. Conf. Develop. Biomed. Eng. Vietnam*, 2020, pp. 383–387.
- [22] A. Dorotić, I. Kuktić, D. Vuljanić, and A.-M. Šimundić, "Verification of technical characteristics and performance of VeinViewer flex, ICEN IN-G090-2 and AccuVein AV400 transillumination devices," *Clinica Chim. Acta*, vol. 519, pp. 40–47, Aug. 2021.
- [23] M. D. Francisco, W.-F. Chen, C.-T. Pan, M.-C. Lin, Z.-H. Wen, C.-F. Liao, and Y.-L. Shiu, "Competitive real-time near infrared (NIR) vein finder imaging device to improve peripheral subcutaneous vein selection in venipuncture for clinical laboratory testing," *Micromachines*, vol. 12, no. 4, p. 373, Mar. 2021.
- [24] C. Tang, S. Xia, M. Qian, and B. Wang, "Deep learning-based vein localization on embedded system," *IEEE Access*, vol. 9, pp. 27916–27927, 2021.
- [25] A. Kuthiala, N. Tuli, H. Singh, O. F. Boyraz, N. Jindal, R. Mavuduru, S. Pattanaik, and P. S. Rana, "U-DAVIS-deep learning based arm venous image segmentation technique for venipuncture," *Comput. Intell. Neurosci.*, vol. 2022, pp. 1–9, Oct. 2022.
- [26] J. Leipheimer, M. Balter, A. Chen, and M. Yarmush, "Design and evaluation of a handheld robotic device for peripheral catheterization," *J. Med. Devices*, vol. 16, no. 2, Jun. 2022, Art. no. 021015.
- [27] S. Biradar, R. G. Talekar, P. N. Yele, G. S. Wable, and P. P. Deshukh, "Non-invasive human vein detector," *Int. Sci. J. Eng. Manag.*, 2023.
- [28] E. Salcedo and P. Peñaloza, "Edge AI-based vein detector for efficient venipuncture in the antecubital fossa," in *Proc. Mexican Int. Conf. Artif. Intell.*, 2023, pp. 297–314.
- [29] N. J. Cuper, J. C. De Graaff, C. J. Kalkman, and R. M. Verdaasdonk, "The vasculuminator: Effectiveness of a near-infrared vessel imaging system as a support in arterial puncture in children," *Adv. Biomed. Clin. Diagnostic Syst.*, vol. 7555, pp. 100–105, 2010.
- [30] *Vein Finder*, China Med. Solution (CMS) Ltd., China, 2018.
- [31] *Vein Viewer ZD200*, Christie Med. Holdings, USA, 2017.
- [32] G. Vt, "A novel design proposal for low-cost vein-viewer for medical and non-contact biometric applications using NIR imaging," *J. Med. Eng. Technol.*, vol. 45, no. 4, pp. 303–312, May 2021.
- [33] *IISM VPism-C Phlebology*, DOTmed, iiSM Inc., South Korea, 2020.
- [34] *Vein Finder V-Pink*, Korrida Med. Syst., 2013.
- [35] *Veineux*, Kerala Medtra Innov. Technol. Pvt Ltd., 2018.
- [36] *Upgraded Vein Locator Medical Light for Venipuncture BS2000+*, Wuxi Belson Med. Syst. Co., Ltd, China, 2012.
- [37] *Vensite Handfree System*, Vuetek Sci., USA, 2013.
- [38] S. Patel, K. P. Bharath, S. Balaji, and R. K. Muthu, "Comparative study on histogram equalization techniques for medical image enhancement," in *Advances in Intelligent Systems and Computing*. Cham, Switzerland: Springer, 2020, pp. 657–669.
- [39] B. C. Grimm, *Imaging, Histogram Equalization*. Scientific Computing and Imagine Institute at the University of Utah.
- [40] K. Singh and R. Kapoor, "Image enhancement using exposure based sub image histogram equalization," *Pattern Recognit. Lett.*, vol. 36, pp. 10–14, Jan. 2014.



GAURAV KUMAR received the Diploma and Bachelor of Technology degrees in computer science engineering from the Thapar Institute of Engineering and Technology, Patiala, India. He has IoT, robotics, drones, AWS, cloud applications, embedded systems, and PCB designing expertise. His major focus areas include the IoMT and the AIoT. He is currently a Research Intern on a project funded by Indian Council of Medical Research, India. He is also a Tech Enthusiast and an Innovator. He runs a website and YouTube channel that features educational videos, for enthusiasts to explore, learn, and build their way to a tech-driven future. He actively shares multiple projects on platforms, such as Arduino and Hackster, contributing to the broader tech community.



HARPREET SINGH received the Ph.D. degree from the Thapar Institute of Engineering and Technology, Patiala, India. He is currently an Assistant Professor with the Computer Science and Engineering Department, Thapar Institute of Engineering and Technology. His research interests include data analytics, machine learning, and deep learning in agriculture and healthcare. He has completed and is currently executing projects as a Project Investigator (PI) and a Co-PI funded by Indian Council of Medical Research, Ministry of Electronics and Information Technology (MEITY), the Government of India, and other funding agencies. He also received the "AROGAYA CIBioD—Innovation and Enterprise Leadership Award" from Indian Council of Medical Research-Centre for Innovation and Bio-Design (ICMR-CIBioD) for his contribution to affordable healthcare. He has published more than 20 research publications in reputed conferences and SCI-indexed journals. He has published and granted various patents in interdisciplinary fields.



PRASHANT SINGH RANA received the Bachelor of Technology degree in information technology stream from Guru Gobind Singh Indraprastha University, Delhi, India, in 2004, and the Master of Technology degree in information technology and the Ph.D. degree in computer science engineering from Indian Institute of Information Technology and Management, Gwalior, India, in 2007 and 2014, respectively. He has been an Associate Professor with the Department of Computer Science and Engineering, Thapar Institute of Engineering and Technology, Patiala, India, since 2021. His areas of specialization include machine learning, data mining, modeling and simulation, parallel algorithms, optimization, and computational biology. He has granted one patent and published nine patents in interdisciplinary fields. He has completed five research projects as a PI or a co-PI and has one ongoing project as a co-PI. He has 56 SCI, 22 conference, and 11 other publications in reputed journals. He is guiding many PG and Ph.D. candidates in the same area. He was an Assistant Professor, from 2015 to 2021, and as a Lecturer for six months with the Department of Computer Science Engineering, Thapar Institute of Engineering and Technology, Patiala, India.



DIVISHA GARG received the Master of Engineering degree in computer science and engineering from Panjab University, Chandigarh, India, in 2019. She is currently pursuing the Ph.D. degree in computer science engineering with the Thapar Institute of Engineering and Technology, Patiala, India. She receives her Junior Research Fellowship from the Department of Urology, Post Graduate Institute of Medical Education and Research, Chandigarh, India. She has been granted one Australian patent. She is executing a project as a Co-Principal Investigator funded by the Council of Scientific and Industrial Research, India. Her research interests include the application of machine learning and image processing in healthcare and agriculture.



SHAHID AHMAD BHAT (Member, IEEE) received the Ph.D. degree in applied mathematics (operations research) from the Thapar Institute of Engineering and Technology, Patiala, India. He is currently a Postdoctoral Researcher with the LUT Business School, LUT University, Finland. Previously, he was a Postdoctoral Fellow with the College of Business and Economics, United Arab Emirates University, Abu Dhabi, United Arab Emirates, for more than one year. He was also an Assistant Professor with the Department of Mathematics, Maharishi Markandeshwar University, India. He has published many reputed research reports in high-impact journals, such as engineering applications of artificial intelligence, applied soft computing, resources policy, and expert systems with applications. His current research interests include the development of an intelligent food supply chain sustainability model based on the Internet of Things (IoT) and artificial intelligence (AI) in the wake of COVID-19 pandemic, optimization techniques, progressive feature extraction of biological sequences for machine learning, fuzzy mathematical model for tumor growth pattern using generalized Hukuhara derivative and its numerical analysis, logistic growth model of tumor population under fuzzy environment and its numerical analysis, and the development of novel multi-attribute decision making (MADM) methods under fuzzy environment and its extensions. He titled some methods for prioritization of alternatives of MADM problems in the fuzzy environment and its extensions.



SMITA PATTANAİK received the Doctorate degree in medicine and in clinical pharmacology. She is currently a Professor in clinical pharmacology with the Post Graduate Institute of Medical Education and Research, Chandigarh, India. She is an Alumnus of the Harvard Medical School with the honor to receive full scholarship and distinction for the GCSRT Program. She is also a Fulbright-Nehru Scholar and completed the program with the Emory University School of Medicine. She is also an Academician and a Researcher, with interests spanning from therapeutic drug monitoring and pharmacogenomics in the clinical pharmacology of immunosuppressives and anticancer drugs. Her focus is translational research, that brings tests and technologies from laboratory to patient use. She has also received many prestigious awards, one such is the Paul Dudley White International Scholar Award. She is a keen learner and active in the global clinical pharmacology communities.



RAVIMOHAN SURYANARAYAN MAVUDURU received the M.B.B.S. degree, in 1999, and the M.Ch. degree in urology from the Post Graduate Institute of Medical Education and Research, Chandigarh, India, in 2007. He is currently a Urologist by profession with 17 years of experience. He is also a Professor in urology with the Post Graduate Institute of Medical Education and Research, Chandigarh.



NEERU JINDAL received the B.Tech. and M.Tech. degrees in electronics and communication from Punjab Technical University, Jalandhar, India, in 2002 and 2007, respectively, and the Ph.D. degree from the Department of Electronics and Communication Engineering, Thapar Institute of Engineering and Technology, Patiala, India, in 2014. She holds the position of an Associate Professor with the Department of Electronics and Communication Engineering, Thapar Institute of Engineering and Technology. She has been involved in various government research projects of DST and ICMR in the area of machine learning and image and video processing. She is a reviewer of many reputed journals and has many granted and published patents. She is guiding many PG and Ph.D. candidates in the same area.

• • •